Applied Physics Letters

Quantum interference in InAs/InAlAs core-shell nanowires

Cite as: Appl. Phys. Lett. **113**, 143104 (2018); https://doi.org/10.1063/1.5049953
Submitted: 26 July 2018 . Accepted: 18 September 2018 . Published Online: 03 October 2018

Y. P. Song, and Y. W. Hu

ARTICLES YOU MAY BE INTERESTED IN

Integrated on-chip silicon plasmonic four quadrant detector for near infrared light
Applied Physics Letters **113**, 143103 (2018); https://doi.org/10.1063/1.5050340

Electrical properties of bulk semi-insulating β-Ga_2O_3 (Fe)
Applied Physics Letters **113**, 142102 (2018); https://doi.org/10.1063/1.5051986

Branched InAs nanowire growth by droplet confinement
Applied Physics Letters **113**, 123104 (2018); https://doi.org/10.1063/1.5045266

AIP Publishing

© 2018 Author(s).

APPLIED PHYSICS LETTERS **113**, 143104 (2018)

Quantum interference in InAs/InAlAs core-shell nanowires

Y. P. Song[1,a)] and Y. W. Hu[2]
[1]*Center for Quantum Information, IIIS, Tsinghua University, Beijing 100084, China*
[2]*Department of Physics, Tsinghua University, Beijing 100084, China*

(Received 26 July 2018; accepted 18 September 2018; published online 3 October 2018)

Ballistic transport of electrons has been experimentally observed in InAlAs/InAs core-shell nanowires. The presence of InAlAs epitaxial shells offers significant improvement to the quality of nanoelectronic devices, leading to the quantum interference in phase coherent electron transport. Regular conductance oscillations are observed due to Fabry-Perot interference by the resonant transmission via quantized states in 1D sub-bands of the InAs nanowire. The simulated transmission of resonance tunneling matches the experimentally observed conductance oscillation patterns, implying the Fabry-Perot interference and ballistic nature of the observed electron transport. *Published by AIP Publishing.* https://doi.org/10.1063/1.5049953

InAs nanowires (NWs) continue to attract much attention as an interesting one-dimensional material for nanoscale circuits,[1] single electron charge sensing,[2] and potentially for spin-based[3] and topological quantum information processing.[4] Electron transport behavior in one-dimensional (1D) quantum wires is of fundamental and practical interest. As the size of a device becomes comparable to the electron coherence length, quantum interference between electron waves becomes increasingly important, resulting in the Fabry-Perot oscillation in ballistic mesoscopic conductors. Such Fabry-Perot interference has been observed in suspended graphene[5] and single-wall nanotubes.[6] However, in InAs nanowires, the disorder and random spatial electrostatic potential have limited the mean free path and prevented the observation of coherence transport.

The intrinsic donor-like surface states of InAs play a major role in determining transport properties,[7] leading to reduced electron mobilities at low temperatures due to the ionized impurity scattering.[8] The charged surface states produce a random spatial electrostatic potential along the nanowire, which may contribute to the spontaneous formation of quantum dots at low temperature.[9] These fluctuations may be due to surface defects,[10] stacking faults,[9] or charge traps in the native oxide layer of the nanowire.[11,12] Fluctuations due to charge traps can vary in time due to carrier trapping and detrapping events, leading to the random telegraph noise (RTN) in the device conductance. We have observed RTN in InAs field-effect transistor (FET) devices and shown results consistent with the charge traps giving rise to RTN residing in the oxide.[12] Surface passivation should reduce the density of ionized surface states and improve the electron mobility of InAs nanowires. Growth of an InP shell on an InAs core has been shown to yield better mobilities,[13] as well as chemical passivation based on In-S bonding.[14,15] We have performed transport measurements on InAs/InAlAs core-shell nanowire FETs and obtained clear evidence for the reduction of ionized impurity scattering in the core-shell nanowires, leading to the highest peak effective mobility of 25 000 cm^2/V s at 1 K that we have not yet observed in an InAs FET device at low temperature.[16] The presence of shell structures in InAs nanowires strongly reduces the random telegraph noise and smoothes out the distortions of the local potential inside the core nanowire. InAlAs epitaxial shells may offer significant improvement to the quality of nanoelectronic devices, leading to the coherence transport in InAs nanowires. In this letter, we report on the observation of quantum interference transport in InAs/InAlAs core-shell nanowires. The simulation of resonance tunneling confirms that conductance oscillations originate from the Fabry-Perot interference and ballistic nature of the electron transport.

Core-shell nanowires were grown in a gas source molecular beam epitaxy (MBE) system using Au seed particles.[17] Transmission electron microscopy (TEM) images of typical nanowires reveal that the nanowires have an inner core and an outer shell structure with low stacking fault densities. Both the core and shell exhibit a wurtzite single-crystal structure. In general, the nanowires had a core diameter of 20–50 nm and a shell that was 10–15 nm thick, independent of the core diameter. The chemical composition of the nanowires was analyzed by energy-dispersive x-ray spectroscopy (EDS). The EDS line scan analysis along the radial direction shows In and As in the core region and In, As, and Al in the shell region with about 20% Al concentration ($In_{0.8}Al_{0.2}As$). Field-effect-transistor devices were fabricated using a standard e-beam lithography technique. As-grown nanowires were mechanically deposited onto a 175 nm thick SiO_2 layer above an n^{++}-Si substrate. Selected nanowires were located relative to pre-fabricated markers by scanning electron microscopy (SEM), with care taken to minimize the electron dose. The contact areas were etched with citric acid to remove the shell material, followed by room temperature sulfur passivation to prevent oxide regrowth during the sample transfer to an e-beam metal evaporator.[34] Ni/Au (30 nm/50 nm) metal contacts were deposited and annealed at 120 °C in vacuum for 10 min to promote Ni diffusion into the nanowire contact area. The device structure is shown schematically in Fig. 1(a), and a SEM image of a typical nanowire FET device is shown in Fig. 1(b). After fabrication, the device chip was wire-bonded into a chip carrier. Transport measurements were

[a)]Author to whom correspondence should be addressed: ypsong@mail.tsinghua.edu.cn

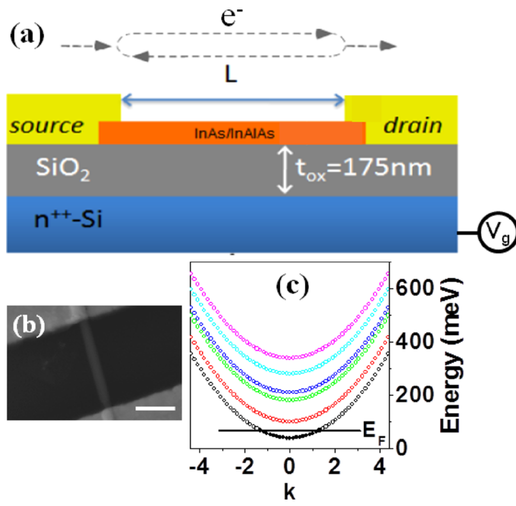

FIG. 1. (a) Schematic cross-section of the FET device. Electrons experience reflections at tunneling barriers leading to Fabry-Perot interference. (b) SEM image of a typical nanowire FET device. The scale bar is 200 nm. The etching profile of the nanowire is seen near the metal contact at the bottom middle. (c) Calculated energy dispersion of the six lowest 1D sub-bands for a NW FET device with diameter $2R_c = 31$ nm and channel length $L = 220$ nm.

carried out in a continuous flow He cryostat operating from 4 to 200 K. Upon applying a DC source-drain voltage V_{sd}, the device current I_{sd} was measured using a current-voltage preamplifier at a noise floor of 0.5 pA $Hz^{1/2}$. A voltage V_g applied to the degenerately doped Si substrate provided a global back gate.

We investigated nearly a dozen devices to varying levels of detail and found qualitatively similar results. Figure 2 shows typical conductance curves versus back-gate voltage for a device measured at 4.6 K with source-drain voltages $V_{sd} = 0.6$ mV, 1.8 mV, and 5.4 mV, respectively. For clarity, the conductance curves at $V_{sd} = 0.6$, 1.8 mV are shifted up. The measured device has a core diameter of 31 nm, a shell diameter of 51 nm, and a channel length of 390 nm, with uncertainties of ± 2 nm. The conductance of core-shell nanowires decreases with decreasing back-gate voltages. The nanowire is fully pinched off below $V_g = 7.28$ V. The important features of the plot are the quasi-period conductance oscillations with a clear dependence of back-gate voltage, superposed with a sequence of changes in oscillation patterns at $V_g = 7.75$, 8.27, 8.59, and 9.08 V, as indicated by four purple arrows in Fig. 2. The amplitude of conductance oscillations reduces with the increase of temperature and smears out when the temperature is above 22 K. To see the quasi-period more clearly, we plot the fast Fourier transform (FFT) for three conductance curves, as shown in the inset in the upper left panel of Fig. 2. The FFT data reveal that three oscillation curves have a similar oscillation period. A peak positioned at 29.8 (1/V) in the FFT plots corresponds to a periodic oscillation of 33.6 mV which dominates the oscillation patterns in Fig. 2.

To clarify these oscillation features, we measured conductance curves by varying the source-drain voltage from -30 mV to 30 mV with a step of 0.6 mV at 4.6 K. The differential conductance dI_{sd}/dV_{sd} is shown in Fig. 3 as a function of the bias voltage V_{sd} and gate voltage V_g. As seen from the figure, the nanowire is pinched off in the regime of $V_g < 7.30$ V. In the regime with higher back gate voltages, quasi-periodic

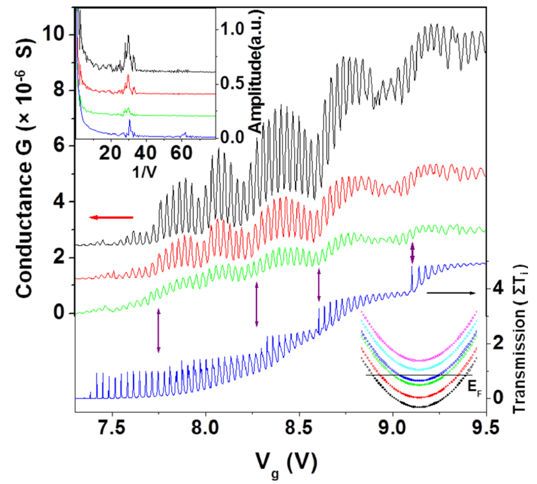

FIG. 2. Conductance oscillations versus back-gate voltage for a device at 4.6 K with a source-drain voltage $V_{sd} = 0.6$ mV (black), 1.8 mV (red), and 5.4 mV (green). For clarity, the conductance curves at $V_{sd} = 0.6$ and 1.8 mV are shifted up 2.45×10^{-6} S and 1.23×10^{-6} S. A sequence of changes in oscillation patterns at $V_g = 7.75$, 8.27, 8.59, and 9.08 V are superposed on the conductance oscillations. The blue curve represents the simulated transmission coefficient with the tunneling barrier $V' = 250$ meV, barrier thickness $l_2 = l_4 = 3$ nm, and channel length $l_3 = 220$ nm. The purple arrows indicate the position where the Fermi level crosses the bottom of the subsequent 1D sub-band. The black arrow indicates the y-axis label of the blue curve on the right side of the figure. The red arrow indicates the y-axis label of the black, red, and blue curves on the left side. The inset shows the fast Fourier transform (FFT) for three experimental conductance curves and the simulated transmission coefficient pattern. The y-axis of the inset represents the amplitude spectrum of the FFT. The plots of FFT in black, red, and green, corresponding to the conductance curves in black, red, and green, are shifted up 0.6, 0.4, and 0.2 y-axis units, respectively.

oscillation patterns are clearly observed. To see these conductance oscillations more clearly, we plot the source-drain current I_{sd} versus back gate V_g in Fig. 4, zooming in the region $V_{sd} = 0.6$–18 mV and $V_g = 7.6$–8.4 V. These conductance oscillations are obviously different from coulomb diamond patterns formed by the coulomb blockade in a quantum dot. For coulomb blockade oscillations, the I_{sd}-V_{sd} curve should show a non-linear (blockade) behavior at the valley of oscillation curves, which is contrast to our observations. Here, I_{sd}-V_{sd} curves show a linear behavior regardless at the peak or valley

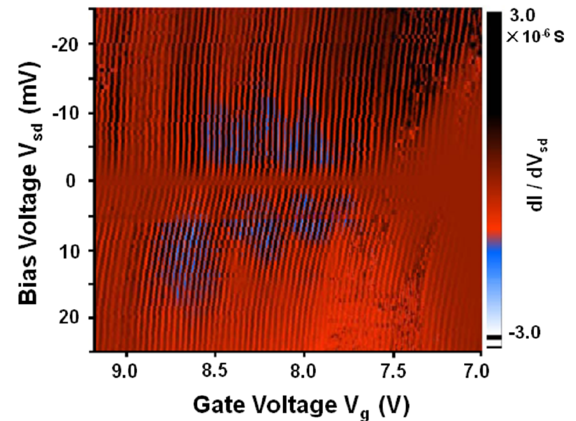

FIG. 3. The differential conductance as a function of the bias voltage and gate voltage by varying the source-drain voltage from -30 mV to 30 mV with a step of 0.6 mV at 4.6 K. The nanowire is pinched off in the regime of $V_g < 7.30$ V, whereas quasi-periodic oscillation patterns are clearly observed in the regime of higher back gate voltages.

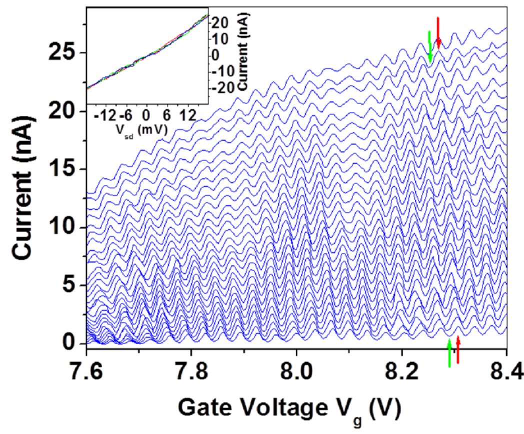

FIG. 4. Source-drain current I_{sd} versus back gate V_g, zooming in the region $V_{sd} = 0.6$–18 mV and $V_g = 7.6$–8.4 V, for the measured device at 4.6 K. The inset shows four I_{sd}-V_{sd} curves extracted from the peak and valley positions of two conductance curves at $V_{sd} = 0.6$ mV and 17.4 mV, as indicated by the red and green arrows. I_{sd}-V_{sd} curves show a linear behavior regardless at the peak or valley position.

position. For instance, as shown in the inset of Fig. 4, four I_{sd}-V_{sd} curves are almost linear, which are extracted from the peak and valley positions of conductance curves, as indicated by the red and green arrows, with $V_{sd} = 0.6$ mV and 17.4 mV, respectively.

Coulomb blockade oscillations seem to be unlikely because the observed oscillations are different from the typical coulomb blockade patterns. Universal conductance oscillations (UCFs) can also be ruled out as a possible origin. UCF origins from electrons being multiply scattered by randomly distributed disorders, result in the random conductance fluctuation with gate voltage.[18,19] Conductance oscillations shown here are in a similar fashion to conductance oscillations observed in ballistic nanotubes due to the quantum interference.[6,20] Hence, a feasible origin of these conductance oscillations is Fabry-Perot-type interference of electrons. Following the method used in the report,[33] we estimated the contact resistance of the measured device. The total resistance of the nanowire device is the sum of the nanowire resistance and of the two contact resistances. It can be expressed as $R = 2R_c + R_q\left(1 + \frac{L}{\lambda}\right)$, where R_c is the contact resistance, R_q is the quantum resistance, L is the channel length, and λ is the electron mean free path in InAs. R_q is $\frac{h}{2e^2}$ (12.91 kΩ) for the 1st sub-band and $\frac{h}{4e^2}$ for the 2nd sub-band due to the degeneracy.[33] The measured resistance of the device is $R = 417.93$ kΩ and 147.51 kΩ, as shown in Fig. 2, when the Fermi level E_F is in the 2nd sub-band and the 4th sub-band at $V_g = 7.894$ V and 8.735 V, respectively. By taking $\lambda \sim 160$ nm (Ref. 33) for the second sub-band and $L = 220$ nm, we can obtain the contact resistance $R_c = 201.30$ kΩ for the 2nd sub-band and $R_c = 69.92$ kΩ for the 4th sub-band. For our device, the etching process for metal contacts could give a constriction in the nanowire between each contact and the unetched part of the nanowire. The etching constrictions may play a crucial role in forming contact barriers. We attribute the high contact resistance to the etching constrictions near the metal contact, the resistance of the nanowire interface to metal leads, together with the non-uniform distribution of the electric field induced by the gate in the vicinity of the source/drain contacts, which are effectively acting as a pair of barriers.[21] We ascribe conductance oscillation phenomena in the core-shell nanowire to the electron resonance tunneling through the contact barriers. Electrons are mostly scattered at the nanowire-metal interface and pass through the nanowire ballistically. Electrons experience reflections at tunneling barriers leading to Fabry-Perot interference, as schematically depicted in Fig. 1(a). The energy dispersion of six lowest 1D sub-bands is calculated using cylindrical coordinates for a NW FET device with diameter $2R_c = 31$ nm and channel length $L = 220$ nm, as shown in Fig. 1(c). The Schrodinger equation can be separated into longitudinal, angular, and radial components ($\varphi_{n,l,z}$). The calculated eigenenergies E_i ($i = 0$–5) corresponding to the bottom edge of 1D sub-bands are 39.91, 101.32, 182.00, 210.26, 280.90, and 339.64 meV, respectively, which are consistent with the experimental sub-band energies for InAs NW devices.[22] As shown in Fig. 1(c), E_F is the Fermi level of the system; the circles refer to the quantized value of k_z implying the limited channel length of the device; and the solid and empty circles relate to occupied and unoccupied states, respectively. The sub-band energy spacing is much larger than the thermal energy k_BT_m (T_m is the measurement temperature), thus, it is safe to treat our NW devices as a 1D system. Constructive interference is expected when $2Lk_F = 2\pi n$, where n is an integer and L is the source-drain channel length. The electron chemical potential, $u = E_F - E_i = \frac{\hbar^2 k_F^2}{2m^*} = \frac{n^2\hbar^2\pi^2}{2m^*L^2}$, is proportional to the gate voltage, $u \propto \alpha V_g$, where E_i is the bottom edge of the corresponding 1D sub-band, m^* is the effective mass, and α is the lever arm of the back gate. Thus, the electron transport can be tuned in and out of the constructive interference, manifesting the electron transmission through the NW and giving rise to conductance oscillations.

Unlike in the case of carbon nanotubes, where transport takes place through the 4-fold degenerate (spin and valley degenerate) 1D sub-bands, the transport in InAs NWs occurs through two 2-fold spin degenerate 1D sub-bands. As the change of Fermi wave vector Δk_F over one period of Fabry-Perot oscillations, the corresponding change in the carrier density in the 1D system, $\Delta n_{1D} = \frac{2\Delta k_F}{\pi} = \frac{2}{L}$, gives $e\Delta n_{1D} = c_g \cdot \Delta V_g$, where c_g is the gate capacitance per unit length and ΔV_g is the oscillation period. Thus, the period of the Fabry-Perot oscillations is directly related to the device channel length $L = \frac{2e}{C_g \cdot \Delta V_g}$.[20,23] c_g can be estimated as the capacitance of a wire above an infinite conducting plane (c'_g) in series with the cylindrical capacitance between the core and shell (c'_s), i.e., $\frac{1}{c_g} = \frac{1}{c'_g} + \frac{1}{c'_s}$. $c'_s = \frac{2\pi\varepsilon_0\varepsilon_{r(shell)}}{\ln\left(\frac{R_s}{R_c}\right)}$, where R_s, R_c is the radius of the nanowire shell and core, respectively. $\varepsilon_{r(shell)}$ is taken as 12.46 for the dielectric constant of the $In_{0.8}Al_{0.2}As$ shell.[24] $c'_g = 2\pi\varepsilon_0\varepsilon_r / \cosh^{-1}\left(\frac{R_s + t_{ox}}{R_s}\right)$, where ε_r is the SiO_2 dielectric constant and t_{ox} is the thickness of the SiO_2 layer.[13,25,26] TEM analysis indicated $t_{ox} = 175$nm. The equation above assumes that the nanowire is embedded in SiO_2. To compensate for the fact that the nanowire actually sits atop the SiO_2 and is surrounded by a vacuum, it was shown by Wunnicke that a modified dielectric constant $\varepsilon_r = 2.2$ can be taken.[25] The calculated gate capacitance per unit length c_g is 43.09 pF/m for a nanowire with

$2R_c = 31$ nm and $2R_s = 51$ nm sitting on the 175 nm oxide layer. Thus, the channel length, calculated from the estimated c_g and oscillations period ΔV_g, is about 224 nm, which is shorter than the physical channel length 390 nm. This deviation may be due to the reduction of channel length by the diffusion of the contact metal into the device channel.[27] The measured device was annealed at 120 °C for 10 min and cooled down afterwards to room temperature in vacuum. It has been reported that contact metal Ni can diffuse into the InAs nanowire to form the Ni_xInAs component during the annealing process.[27] The diffusion length increases with increasing the annealing time. By SEM imaging at a high acceleration voltage of electron beam, some contrasts can be seen between the bare nanowire section and metal diffusion section for the devices annealed at 120 °C for 30 min. The Ni contact metal diffuses into the device channel around 150–220 nm, varying from device to device. The diffusion length is estimated to be 80–110 nm for the devices annealed at 120 °C for 10 min, according to the relation of the diffusion length to the annealing time.[27] Thus, the effective channel length can be shortened by the diffusion of Ni into the channel.

These Fabry-Perot conductance oscillations can also be interpreted as resonant tunneling via virtual states with energy spacing ΔEz, as schematically shown in Fig. 1(c). The quantized values of k_z calculated in the figure refer to the device channel length of 220 nm. The conductance of resonance tunneling can thus be calculated according to the Fermi energy of the system and the tunneling barriers formed in the channel regime of the device. The electron charge in the 1D nanowire, $n_{1D} = \frac{2\sqrt{2m^*}}{\pi\hbar}\sum_i \sqrt{E_F - E_i}$,[20,22] is related to the gate voltage by $n_{1D} = c_g(V_g - V_{th})/e$, for all populated sub-bands with energies less than the Fermi level E_F. Here, E_i is the ith sub-band edge energy, and $m = 0.023m_0$ is the InAs electron effective mass used in the simulations, c_g is the gate capacitance per unit length, and V_{th} is the threshold voltage. As shown in Fig. 2, the nanowire is fully pinched off when the gate voltage is below 7.28 V, so we can consider a threshold voltage of 7.28 V. With respect to the nanowire with $2R_c = 31$ nm and the effective channel length of 220 nm, we estimated the carrier density to be 2.2×10^{17} cm^{-3} in the nanowire at $V_g = 7.894$ V. The Fermi level can thus be extracted from the charge density which is modulated by the gate voltage through the populated 1D sub-bands. The transmission coefficient can be readily obtained with the method based upon the analogy between the transmission-line theory and quantum mechanics.[28,29] By impedance-matching the plane wave solutions of the Schrodinger equation at appropriately chosen potential discontinuities, the transmission coefficient T_i associated with the i-th mode can be determined. The total conductance through the nanowire is related to the transmission coefficient with multiple modes by the two-terminal Landauer-Buttiker formula $G = \frac{2e^2}{\hbar}\sum_i T_i$.[20] The blue curve shown in Fig. 2 represents the simulated transmission coefficient with the tunneling barrier $V' = 250$ meV, barrier thickness $l_2 = l_4 = 3$ nm, and channel length $l_3 = 220$ nm. The purple arrows indicate the position where the Fermi level crosses the bottom of the subsequent 1D sub-band. The simulated transmission matches the conductance oscillation pattern well. The fast Fourier transform (FFT) of the transmission curve, as shown as the blue curve in the inset of Fig. 2, reveals a periodic oscillation of 33.2 mV [30.12 (1/V)], which is close to the oscillation period of experimental conductance curves (33.6 mV). A sequence of changes in the transmission curves occurs when the Fermi level crosses the bottom of the subsequent 1D sub-band[30] at 39.91, 101.32, 182.00, 210. and 280.90 meV, respectively, matching the trend of changes in the conductance oscillation curves observed experimentally. We calculated transmission coefficients with varying simulation parameters of the barrier height, barrier thickness, and channel length. The results are shown in Fig. S2 in the supplementary material. It is worth noting that the tunneling barriers are crucial to observe the quantum interference. The increase of the width and height of tunneling barriers reduces the transmission coefficient significantly, but only modulates the oscillation period slightly. The change of channel length, however, results in an obvious change in the oscillation period. The optimal channel length inferred from simulations is about 220 nm, which is quite close to the value estimated from the Fabry-Perot interference model (224 nm). The oscillation period yielded from simulations with a deviation of channel length does not match the experimental period any more, regardless of what reasonable parameters of barrier height and thickness are used for simulations. This made us believe that the real effective channel length must be close to 220 nm. This agreement further confirms the hypothesis that the conductance oscillation originates from the Fabry-Perot interference with the resonant transmission via quantized states in 1D sub-bands of the InAs nanowire.

The electron transport should be ballistic within the effective channel length of the nanowire device, otherwise, the carriers would be scattered randomly leading to the randomization of the phase and smearing of Fabry-Perot oscillations. Previous studies of ballistic transport in InAs nanowires have observed a mean free path around 200 nm.[31–33] This mean free path is of the order of the effective channel length in our NW device. It is worth noting that these conductance oscillations have been only observed in InAs/InAlAs core-shell nanowires; no similar phenomenon has been found in bare InAs nanowires. The random spatial electrostatic potentials along the nanowire, due to surface defects,[10] stacking faults,[9] or charge traps,[11,12] scatter electrons and smear out the ballistic transport in bare InAs nanowires. Surface passivation of shell structures for InAs nanowires smoothes out the distortions of the local potential inside the core nanowire, leading to ballistic transports in InAs nanowires. Indeed, ballistic transport has been observed in the suspended InAs NW device, while conventional unsuspended geometry exhibited random switchings and hysteresis of gate dependence regardless of the crystalline quality of the NWs.[21] All these indicate that the reduction of random surface potentials is crucial to observe the ballistic transport with phase coherence in InAs nanowires.

In summary, we performed experimental measurements of ballistic transport in InAlAs/InAs core-shell nanowires. A serious impediment to obtaining clean behavior in transport devices is the uncontrolled spatial variation of electrostatic potential along the channel of transport. By reducing the

random telegraph noise and smoothing out the distortions of local potential inside the core nanowire, the presence of InAlAs epitaxial shells offers significant improvement to the quality of nanoelectronic devices, leading to the quantum interference in phase coherent electron transport. Ballistic transport of electrons has been experimentally observed in InAs/InAlAs core-shell nanowires. Regular conductance oscillations are observed due to the Fabry-Perot interference by the resonant transmission via quantized states in 1D subbands of the InAs nanowire. The simulated transmission of resonance tunneling matches the experimentally observed conductance oscillation patterns, implying the Fabry-Perot interference and ballistic nature of the observed electron transport.

See supplementary material for the etching method and the calculation of transmission coefficients with varying simulation parameters of barrier height, barrier thickness, and channel length.

This work was supported by the National Natural Science Foundation of China under Grant No. 11874235 and the State's Key Project of Research and Development Plan under Grant No. 2016YFA0301902.

[1]S. Nam, X. Jiang, Q. Xiong, D. Ham, and C. M. Lieber, Proc. Natl. Acad. Sci. U.S.A. **106**, 21035 (2009).
[2]J. Salfi, I. G. Savelyev, M. Blumin, S. V. Nair, and H. E. Ruda, Nat. Nanotechnol. **5**, 737 (2010).
[3]S. Nadj-Perge, S. M. Frolov, E. P. A. M. Bakkers, and L. P. Kouwenhoven, Nature **468**, 1084 (2010).
[4]V. Mourik, K. Zuo, S. M. Frolov, S. R. Plissard, E. P. A. M. Bakkers, and L. P. Kouwenhoven, Science **336**, 1003 (2012).
[5]P. Rickhaus, R. Maurand, M. H. Liu, M. Weiss, K. Richter, and C. Schönenberger, Nat. Commun. **4**, 2342 (2013).
[6]J. Kong, E. Yenilmez, T. W. Tombler, W. Kim, and H. J. Dai, Phys. Rev. Lett. **87**, 106801 (2001).
[7]S. A. Dayeh, Semicond. Sci. Technol. **25**, 024004 (2010).
[8]N. Gupta, Y. P. Song, G. W. Holloway, U. Sinha, C. M. Haapamaki, R. R. LaPierre, and J. Baugh, Nanotechnology **24**, 225202 (2013).
[9]M. D. Schroer and J. R. Petta, Nano Lett. **10**, 1618 (2010).
[10]S. A. Dayeh, C. Soci, P. K. L. Yu, E. T. Yu, and D. Wang, J. Vac. Sci. Technol., B **25**, 1432 (2007).
[11]J. Salfi, S. V. Nair, I. G. Savelyev, M. Blumin, and H. E. Ruda, Phys. Rev. B **85**, 235316 (2012).
[12]G. W. Holloway, Y. P. Song, C. M. Haapamaki, R. R. LaPierre, and J. Baugh, J. Appl. Phys. **113**, 024511 (2013).
[13]J. W. W. van Tilburg, R. E. Algra, W. G. G. Immink, M. Verheijen, E. P. A. M. Bakkers, and L. P. Kouwenhoven, Semicond. Sci. Technol. **25**, 024011 (2010).
[14]M. H. Sun, H. J. Joyce, Q. Gao, H. H. Tan, C. Jagadish, and C. Z. Ning, Nano Lett. **12**, 3378 (2012).
[15]Q. Hang, F. Wang, P. D. Carpenter, D. Zemlyanov, D. Zakharov, E. A. Stach, W. E. Buhro, and D. B. Janes, Nano Lett. **8**, 49 (2008).
[16]G. W. Holloway, Y. P. Song, C. M. Haapamaki, R. R. LaPierre, and J. Baugh, Appl. Phys. Lett. **102**, 043115 (2013).
[17]M. C. Plante and R. R. LaPierre, J. Appl. Phys. **105**, 114304 (2009).
[18]Y.-J. Doh, A. L. Roest, E. P. A. M. Bakkers, S. De Franceschi, and L. P. Kouwenhoven, J. Korean Phys. Soc. **54**, 135 (2009).
[19]T. S. Jespersen, M. L. Polianski, C. B. Sorensen, K. Flensberg, and J. Nygård, New J. Phys. **11**, 113025 (2009).
[20]W. J. Liang, M. Bockrath, D. Bozovic, J. H. Hafner, M. Tinkham, and H. Park, Nature **411**, 665 (2001).
[21]A. V. Kretinin, R. P. Biro, D. Mahalu, and H. Shtrikman, Nano Lett. **10**, 3439 (2010).
[22]A. C. Ford, S. B. Kumar, R. Kapadia, J. Guo, and A. Javey, Nano Lett. **12**, 1340 (2012).
[23]M. J. Biercuk, N. Mason, J. Martin, A. Yacoby, and C. M. Marcus, Phys. Rev. Lett. **94**, 026801 (2005).
[24]M. A. Littlejohn, K. W. Kim, and H. Tian, "High-field transport in InGaAs and related heterostructures," in *Properties of Lattice-Matched Strained Indium Gallium Arsenide*, edited by P. Bhattacharya (Inspec, IEE, London, 1993), Sec. 4.2, pp. 107–116.
[25]O. Wunnicke, Appl. Phys. Lett. **89**, 083102 (2006).
[26]C. F. Alexandra, C. H. Johnny, Y. L. Chueh, Y. C. Tseng, Z. Y. Fan, J. Guo, J. Bokor, and A. Javey, Nano Lett. **9**, 360 (2009).
[27]Y. L. Chueh, C. F. Alexandra, C. H. Johnny, Z. A. Jacobson, Z. Y. Fan, C. Y. Chen, L. J. Chou, and A. Javey, Nano Lett. **8**, 4528 (2008).
[28]A. N. Khondker, M. R. Khan, and A. F. M. Anwar, J. Appl. Phys. **63**, 5191 (1988).
[29]F. M. de Aguiar and D. A. Wharam, Phys. Rev. B **43**, 9984 (1991).
[30]A. Sa'ar, J. Feng, I. Gravé, and A. Yariv, J. Appl. Phys. **72**, 3598 (1992).
[31]X. Zhou, S. A. Dayeh, D. Aplin, D. Wang, and E. T. Yu, J. Vac. Sci. Technol., B **24**, 2036 (2006).
[32]S. A. Dayeh, D. Susac, K. L. Kavanagh, E. T. Yu, and D. L. Wang, Nano Lett. **8**, 3114 (2008).
[33]S. Chuang, Q. Gao, R. Kapadia, A. C. Ford, J. Guo, and A. Javey, Nano Lett. **13**, 555 (2013).
[34]D. B. Suyatin, C. Thelander, M. T. Björk, I. Maximov, and L. Samuelson, Nanotechnology **18**, 105307 (2007).